INTERNATIONAL JOURNAL FOR NUMERICAL METHODS IN ENGINEERING
Int. J. Numer. Meth. Engng 2011; **85**:896–919
Published online 23 August 2010 in Wiley Online Library (wileyonlinelibrary.com). DOI: 10.1002/nme.3006

Advanced fully coupled thermo-mechanical plate elements for multilayered structures subjected to mechanical and thermal loading

P. Nali[1,*,†,‡], E. Carrera[1,§] and A. Calvi[2,¶]

[1]*Aerospace Department, Politecnico di Torino, Corso Duca degli Abruzzi, 24, 10129 Torino, Italy*
[2]*ESA/ESTEC, P.O. Box 299, Noordwijk 2200 AG, The Netherlands*

SUMMARY

This paper presents a hierarchical modeling for the analysis of multilayered structures subjected to mechanical and thermal loadings. The principle of virtual displacement is applied in the framework of the Carrera unified formulation to obtain a complete family of plate finite elements. The order of the variable description through the plate-thickness direction can be set in the range from one to four. The results in the form of tables and graphs are given to validate the proposed elements. Pure mechanical and fully coupled thermo-mechanical cases studies are proposed. The application of Fourier's law is not required since the plate-thickness temperature profile is automatically obtained in the framework of the proposed approach. The numerical results are obtained through the *MUL2* academic code. Copyright © 2010 John Wiley & Sons, Ltd.

Received 19 April 2010; Revised 25 June 2010; Accepted 28 June 2010

KEY WORDS: multifield problems; thermo-mechanical coupling; plate finite elements; modeling of multilayered plates

1. INTRODUCTION

Thermo-mechanical coupling effects play a crucial role in the operational life of aerospace structures. They often represent the main cause of failure and as a consequence they should be considered in the earlier stages of the design process. Thin-walled parts of reactor vessels, turbines and the structures of future supersonic and hypersonic vehicles (such as high-speed civil transport and advanced tactical fighters) are particularly susceptible to failure resulting from an excessive stress level induced by thermal or combined thermo-mechanical loadings [1]. Thermal deformation also plays a fundamental role in multilayered thin-film zones, comprising optical mirrors [2], as well as space reflector antennas, which require stringent geometric tolerance compared with the traditional structures [3].

The present research paper is restricted to plate geometries. Early [4, 5] and recent [2, 6, 7] exact three-dimensional solutions have shown that appropriate structural modelings are required to meet the C_z^0-requirements summarized in work [8]: in order to account for zig-zag effects and interlaminar continuity, both displacement and transverse stress field must be C_z^0-continuous

*Correspondence to: P. Nali, Aerospace Department, Politecnico di Torino, Corso Duca degli Abruzzi, 24, 10129 Torino, Italy.
†E-mail: pietro.nali@polito.it
‡PhD.
§Professor.
¶Senior Scientist.

functions in the plate-thickness direction. Many papers have proposed and applied the classical and advanced theories on this topic. The following conclusion has been reached by Murakami [2]: 'in order to predict rapid variation of transverse normal strains, a plate theory with cubic variation of in-plane displacement in each layer, rather than over the entire plate thickness should be adopted. Otherwise full three-dimensional analyses are recommended'. In other words, due to the intrinsic through-the-thickness variation of thermal loadings, a layer-wise (LW) kinematic variable description is required to accurately calculate the local response of layered plates. Another more simple and less accurate description is represented by the equivalent single layer (ESL) approach. The conclusion recently reached by Bhaskar and Varadan [9], who underline the importance of refined theories to handle thermal loadings accurately with respect to mechanical ones, is also relevant.

A lot of commercial software is available, which solves thermo-mechanical problems by employing the finite element method (FEM) and using solid finite elements (FEs). These codes are *partially coupled* in that they can furnish the mechanical deformation subsequent to a thermal loading, but do not permit the thermal variation caused by a mechanical loading (an effect that is almost always negligible) to be calculated. Moreover, solid elements are particularly inconvenient when multilayered structures have to be analyzed. In fact, at least three solid element should be placed through the thickness of each layer to have reasonable results and this leads to heavy computational costs. It is implicit that the use of plate elements instead of solid elements would decrease the number of DOFs involved in the analysis.

In this paper, plate thermo-mechanical FEs are obtained according to the Carrera unified formulation (CUF) [10]. Only in-plane stress the results are listed in the following since the exact solution for transverse stresses is not available in the reference work [11]. However, the full three-dimensional state of stress, including all transverse stress components, is required in case of failure analysis of composite multilayered structures. Additional information on this topic can be found in works [12–14]. The FEs presented here are *fully-coupled*: if a mechanical loading is applied to the structure, the temperature variation caused by mechanical deformations can be calculated as an instantaneous effect. This last point is crucial when thermographic experiments are conducted to recover the three-dimensional stress field starting from a temperature distribution [15, 16]. There are some other rare cases when the coupled interaction from mechanical to thermal field can be significant. This is the case of heat dissipation processes or large thermo-mechanical excitations that can be found in forming processes.

Analytical solutions for the stress analysis of multilayered plates subjected to thermal loading were proposed in work [17], with particular emphasis on stress field calculation referring to the principle of virtual displacement (PVD) and Reissner's mixed variational theorem (RMVT) variational statements. The corresponding plate FEs were proposed in works [18] and [19], respectively for PVD and RMVT applications. The effects of the thermo-mechanical full coupling were briefly presented in the previous work [20]. Fourier's law was applied to calculate the plate-thickness steady-state temperature profile in the previous works.

The aim of this work is to illustrate the advantages of the proposed hierarchical plate thermo-mechanical FEs. It is specified that, after some enhancements in the formulation, the additional application of Fourier's law is not required to obtain the plate-thickness steady-state temperature profile, which is calculated together with the other primary unknowns, in one single analysis. The final user can choose the kinematic description (ESL or LW) and the order of the through-the-thickness polynomial expansion, ranging from one to four.

Apropos of thermo-mechanical coupling, following remark should be done. The application of Fourier's law usually requires a minimum computational effort and thus the fully coupled approach does not increase the computational efficiency of the solver, leading only to the practical advantage that the number of analysis to be performed passes from two to one. Nevertheless, there some other cases in which the fully coupling leads also to numerical advantages. It is the case of functionally graded materials (FGM) plate modeling. In fact, depending on the law describing the FGM properties through the thickness of the plate, the calculation of the thickness temperature profile via Fourier's law could be challenging and not immediate. In contrary, if

DOI: 10.1002/nme

the fully coupled interactions are included in the modeling, the thickness temperature profile is automatically calculated (FEs for FGM modeling are currently under validation and they will appear in a future work).

The first part of this paper is focused on the description of the necessary methodology to obtain the coupled FE matrices for multilayered plate two-dimensional modeling. The PVD is applied. The second part is devoted to several benchmarks, which assess the capabilities of the proposed FEs for pure mechanical and thermo-mechanical problems. Moreover, the relevance of higher-order effects in the stress field calculation is quantified through comparisons with exact solutions. Linear static and dynamic results are discussed.

2. CONSTITUTIVE EQUATIONS FOR THERMO-MECHANICAL PROBLEMS

The constitutive equations are obtained, in this section, in the linear case for the fully coupled thermo-mechanical analysis. The standard tensor notation is used and Einstein's summation convention is implied over repeated indices. A cartesian reference system is considered. The intensive variables θ and ε, which are respectively the increment in temperature with respect to the reference temperature θ_{ref} and the strains, are considered as independent variables. The relevant thermodynamic functions are the Gibbs free energy-per-unit of volume G [21], the dissipation F and the thermo-mechanical enthalpy density H:

$$G(U, \varepsilon_{ij}, \theta) = U + \sigma_{ij}\varepsilon_{ij} - \eta\theta, \tag{1}$$

$$F(\vartheta_i) = \tfrac{1}{2}\kappa_{ij}\vartheta_i\vartheta_j - \tau_0\dot{q}_i, \tag{2}$$

$$H(U, \varepsilon_{ij}, \theta, \vartheta_i) = G - F, \tag{3}$$

where:

$U =$ internal energy per unit of volume;
$\sigma_{ij} =$ stress tensor;
$\eta =$ variation of entropy per unit of volume;
$\kappa_{ij} =$ conductivity tensor;
$\vartheta_i =$ heat strain vector;
$\tau_0 =$ thermal relaxation parameter;
$\dot{q}_i =$ temporal derivative of the heat flux q_i.

Then, the dissipation function F has to be used only if a certain temperature is imposed on the surfaces of the structure and the steady-state temperature profile needs to be calculated. Differently, if the interest is in the instantaneous temperature profile caused by a mechanical deformation, the contribution of F has to be neglected [22]. The temporal derivative of the heat flux is set to zero in the present work since only stationary fluxes are considered as the boundary conditions.

The Gibbs free energy can be written as a quadratic form according to [21]:

$$G = \frac{1}{2}\left(\theta^2\frac{\partial^2 G}{\partial\theta^2} + \varepsilon_{ij}\varepsilon_{lm}\frac{\partial^2 G}{\partial\varepsilon_{ij}\partial\varepsilon_{lm}} + \theta\varepsilon_{lm}\frac{\partial^2 G}{\partial\theta\partial\varepsilon_{lm}} + \varepsilon_{ij}\theta\frac{\partial^2 G}{\partial\varepsilon_{ij}\partial\theta}\right). \tag{4}$$

Consequently, H takes the following form:

$$H = \frac{1}{2}\left(\theta^2\frac{\partial^2 H}{\partial\theta^2} + \varepsilon_{ij}\varepsilon_{lm}\frac{\partial^2 H}{\partial\varepsilon_{ij}\partial\varepsilon_{lm}} + \theta\varepsilon_{lm}\frac{\partial^2 H}{\partial\theta\partial\varepsilon_{lm}} + \varepsilon_{ij}\theta\frac{\partial^2 H}{\partial\varepsilon_{ij}\partial\theta} - \kappa_{ij}\vartheta_i\vartheta_j\right). \tag{5}$$

DOI: 10.1002/nme

The exact differential of H is

$$\mathrm{d}H = \sigma_{ij}\mathrm{d}\varepsilon_{ij} - \eta\mathrm{d}\theta - q_i\mathrm{d}\vartheta_i, \tag{6}$$

where:

$$\sigma_{ij} = \left[\frac{\partial H}{\partial \varepsilon_{ij}}\right]_\theta, \quad \eta = -\left[\frac{\partial H}{\partial \theta}\right]_\varepsilon, \quad q_i = \left[\frac{\partial H}{\partial \vartheta_i}\right]. \tag{7}$$

Subscripts refer to the quantities to be kept constant in the differentiation.

Substituting Equation (5) into Equation (7) one has:

$$\sigma_{ij} = \theta\left[\frac{\partial^2 H}{\partial \varepsilon_{ij}\partial\theta}\right] + \varepsilon_{ij}\left[\frac{\partial^2 H}{\partial \varepsilon_{ij}\partial\varepsilon_{lm}}\right]_\theta. \tag{8}$$

$$\eta = \theta\left[-\frac{\partial^2 H}{\partial\theta^2}\right]_\varepsilon + \varepsilon_{ij}\left[-\frac{\partial^2 H}{\partial\theta\partial\varepsilon_{ij}}\right]; \tag{9}$$

$$q_i = \vartheta_i\left[-\frac{\partial^2 H}{\partial\vartheta_i\partial\vartheta_j}\right]. \tag{10}$$

The following coefficients are so defined

$$\begin{aligned} C^\theta_{ijlm} &= \left[\frac{\partial^2 H}{\partial\varepsilon_{ij}\partial\varepsilon_{lm}}\right]_\theta = \left[\frac{\partial\sigma_{ij}}{\partial\varepsilon_{lm}}\right]_\theta, \\ \frac{\rho C^\varepsilon}{\theta_{\mathrm{ref}}} &= -\left[\frac{\partial^2 H}{\partial\theta^2}\right]_\varepsilon = \left[\frac{\partial\eta}{\partial\theta}\right]_\varepsilon, \\ \lambda_{ij} &= -\left[\frac{\partial^2 H}{\partial\theta\partial\varepsilon_{ij}}\right] = \left[\frac{\partial\sigma_{ij}}{\partial\theta}\right]_\varepsilon = \left[\frac{\partial\eta}{\partial\varepsilon_{ij}}\right]_\theta, \\ \kappa_{ij} &= -\left[\frac{\partial^2 H}{\partial\vartheta_i\partial\vartheta_j}\right] = -\left[\frac{\partial q_i}{\partial\vartheta_j}\right], \end{aligned} \tag{11}$$

with:

C_{ijlm} = elastic coefficients—Hooke's law;
ρ = density;
$C^{\varepsilon,E,H}$ = specific heat per unit mass;
λ_{ij} = stress-temperature coefficients.

The first two constants in Equations (11) are principal constants in the respective individual systems; the third one is the coupling constant between the two considered fields. Introducing the constants of Equations (11), the following constitutive equations in the fully coupled two-field system are obtained by Equations (8)–(10):

$$\begin{aligned} \sigma_{ij} &= -\lambda_{ij}\theta + C^\theta_{ijlm}\varepsilon_{lm}, \\ \eta &= \frac{\rho}{\theta_{\mathrm{ref}}}C^\varepsilon\theta + \lambda_{ij}\varepsilon_{ij}, \\ q_i &= \kappa_{ij}\vartheta_j. \end{aligned} \tag{12}$$

DOI: 10.1002/nme

As emphasized in [21], physical constants are introduced by the second derivative of the relevant thermodynamic function. The coupling constant is a second derivative with respect to two different variables, and is therefore considered to have a different meaning when interchanging the order of differentiation:

$$\lambda_{ij}=\left[\frac{\partial\sigma_{ij}}{\partial\theta}\right]_{\varepsilon} \quad \text{and} \quad \lambda_{ij}=\left[\frac{\partial\eta}{\partial\varepsilon_{ij}}\right]_{\theta}.$$

The former λ represents the stress variation versus unit temperature, whereas the latter λ represents the entropy variation versus unit strain. The equality of those effects is thus self-evident.

2.1. PVD—principle of virtual displacements

In this section, the PVD is derived according to the constitutive relations and neglecting the dissipation function that will be introduced later. It is convenient to start the derivation directly from Hamilton's principle

$$\delta\int_{t_0}^{t}(K-\Pi)\,\mathrm{d}t=0\Rightarrow\delta\int_{t_0}^{t}K\,\mathrm{d}t-\delta\int_{t_0}^{t}\Pi\,\mathrm{d}t=0, \tag{13}$$

where K is the kinetic energy and Π is the potential energy; δ is the variational symbol; t denotes time, t_0 and t_1 are the initial and generic instants. The kinetic energy variation can be treated as follows:

$$\begin{aligned}\delta\int_{t_0}^{t}K\,\mathrm{d}t&=\delta\int_{t_0}^{t}\mathrm{d}t\int_{V}\left(\frac{1}{2}\rho\dot{u}_i\dot{u}_i\right)\mathrm{d}V=\int_{t_0}^{t}\int_{V}\rho\dot{u}_i\delta\dot{u}_i\,\mathrm{d}V\,\mathrm{d}t\\&=\int_{V}\rho\dot{u}_i\delta u_i\,\mathrm{d}V\Big|_{t_0}^{t_1}-\int_{t_0}^{t_1}\int_{V}\rho\ddot{u}_i\delta u_i\,\mathrm{d}V\,\mathrm{d}t.\end{aligned} \tag{14}$$

V is the plate volume, u_i is a displacement component and dot denotes differentiation with respect to time. δu is equal zero in $t=t_0$ and $t=t_1$, so that:

$$\delta\int_{t_0}^{t}K\mathrm{d}t=-\int_{t_0}^{t_1}\int_{V}\rho\ddot{u}_i\delta u_i\,\mathrm{d}V\,\mathrm{d}t. \tag{15}$$

It follows that:

$$\delta\int_{t_0}^{t}K\mathrm{d}t=-\int_{t_0}^{t}\delta L_{\mathrm{in}}\,\mathrm{d}t, \tag{16}$$

in which δL_{in} denotes the variation of the work done by inertial forces.

The variation of potential energy is written as an algebraic sum of the variation of H and the variation of the work made the applied mechanical loading (e.g. a pressure).

$$\delta\int_{t_0}^{t}\Pi\,\mathrm{d}t=\delta\int_{t_0}^{t}\left[\int_{V}H\,\mathrm{d}V-\int_{A}(\bar{t}_j u_j)\mathrm{d}A\right]\mathrm{d}t=\delta\int_{t_0}^{t}\int_{V}H\,\mathrm{d}V\,\mathrm{d}t-\int_{t_0}^{t}\delta L_e\,\mathrm{d}t, \tag{17}$$

where:

A is the surface involved by loading;
$\bar{t}_j$ is the pressure in j-direction;
δL_e denotes the variation of the work done by external loads.

Substituting Equations (16) and (17) into Equation (13), it follows that:

$$\delta\int_{t_0}^{t}\int_{V}H\,\mathrm{d}V\,\mathrm{d}t=\int_{t_0}^{t}\delta L_e\,\mathrm{d}t-\int_{t_0}^{t}\delta L_{in}\,\mathrm{d}t. \tag{18}$$

DOI: 10.1002/nme

Differentiating the enthalpy density, Equation (18) takes the following form:

$$\int_{t_0}^{t}\int_V \left(\frac{\partial H}{\partial \varepsilon_{ij}}\delta\varepsilon_{ij}+\frac{\partial H}{\partial \theta}\delta\theta\right)\mathrm{d}V\,\mathrm{d}t=\int_{t_0}^{t}\delta L_e\,\mathrm{d}t-\int_{t_0}^{t}\delta L_{\mathrm{in}}\,\mathrm{d}t. \tag{19}$$

Substituting Equation (7) intp Equation (19), neglecting the dissipation function and eliminating the time integral, the PVD for a three-dimensional continua is obtained as

$$\int_V(\sigma_{ij}\delta\varepsilon_{ij}-\eta\delta\theta)\,\mathrm{d}V=\delta L_e-\delta L_{\mathrm{in}}. \tag{20}$$

Passing from indices to vectors, the following condensed notation can be introduced. It is useful to collect vectors $\boldsymbol{\sigma}, \eta$ and $\boldsymbol{\epsilon}, \theta$ in $\mathscr{E}$ and $\mathscr{S}$ respectively; $\mathscr{S}$ is the vector of extensive variables while $\mathscr{E}$ is the vector of intensive ones (bold letters denote arrays and ε_{ij} components in the vectorial notation correspond to $2\varepsilon_{ij}$ components in tensorial notation, when $i\neq j$):

$$\mathscr{S}^{\mathrm{T}}=\{\sigma_{xx}\ \ \sigma_{yy}\ \ \sigma_{xy}\ \ -\eta\ \ \sigma_{zz}\ \ \sigma_{xz}\ \ \sigma_{yz}\}, \tag{21}$$

$$\mathscr{E}^{\mathrm{T}}=\{\varepsilon_{xx}\ \ \varepsilon_{yy}\ \ \varepsilon_{xy}\ \ \theta\ \ \varepsilon_{zz}\ \ \varepsilon_{xz}\ \ \varepsilon_{yx}\}. \tag{22}$$

Note that dealing with plates, subscript 'z' indicates the through-the-thickness z-direction while subscripts 'x' and 'y' are for the two in-plane directions. The non-mechanical quantity η appears under negative sign in vector $\mathscr{S}$ and this is in accordance with Equation (1). In doing so, the PVD statement for a multilayered plate results in the following compact form:

$$\int_V(\delta\mathscr{E}_G^{\mathrm{T}}\mathscr{S}_H)\,\mathrm{d}V=\delta L_e-\delta L_{\mathrm{in}}, \tag{23}$$

where subscripts 'G' and 'H' indicate variables obtained by Geometrical relations and by constitutive/Hooke's relations, respectively. For multilayered structures, the volume integral, has to be intended as:

$$\int_V(\ldots)\,\mathrm{d}V=\sum_{k=1}^{N_l}\int_{\Omega_k}\int_{h_k}t(\ldots)\,\mathrm{d}\Omega_k\,\mathrm{d}z, \tag{24}$$

where Ω_k is the middle layer surface, k indicates the kth layer of the plate and h_k denotes the kth layer-thickness domain.

3. FE EQUATIONS IN TERMS OF 'FUNDAMENTAL NUCLEI' FOR MULTILAYERED STRUCTURES

3.1. Geometrical relation

$\boldsymbol{U}^k$ denotes the vector containing primary unknowns of the problem. The superscript T indicates the array transposition. Note that displacements and temperature variables are collected together in vector $\boldsymbol{U}^k$. A suitable choice for PVD application is:

$$\boldsymbol{U}^{k\mathrm{T}}=\{u_x^k\quad u_y^k\quad u_z^k\quad \theta^k\}. \tag{25}$$

The intensive variables $\mathscr{E}^k$ are linearly related to the unknowns $\boldsymbol{U}^k$ according to the following geometrical relations:

$$\mathscr{E}_G^k=\boldsymbol{D}\boldsymbol{U}^k, \tag{26}$$

DOI: 10.1002/nme

where $\boldsymbol{D}$ denotes the following differential operator:

$$\boldsymbol{D}=\begin{pmatrix} \partial_x & 0 & 0 & 0 \\ 0 & \partial_y & 0 & 0 \\ \partial_y & \partial_x & 0 & 0 \\ 0 & 0 & 0 & 1 \\ 0 & 0 & \partial_z & 0 \\ \partial_z & 0 & \partial_x & 0 \\ 0 & \partial_z & \partial_y & 0 \end{pmatrix}. \tag{27}$$

3.2. Constitutive relations

The geometry and Cartesian coordinate system x, y, z of the multilayered plates made of N_l layers are those of Figure 1. The lamina are considered to be homogeneous and to operate in the linear elastic range. Material is assumed to be orthotropic. Constitutive coefficient can be organized in matrix $\boldsymbol{H}^k$:

$$\mathscr{S}^k_H=\boldsymbol{H}^k\mathscr{E}^k_G, \tag{28}$$

where:

$$\boldsymbol{H}^k=\begin{pmatrix} C^k_{11} & C^k_{12} & C^k_{16} & -\lambda^k_1 & C^k_{13} & 0 & 0 \\ C^k_{12} & C^k_{22} & C^k_{26} & -\lambda^k_2 & C^k_{23} & 0 & 0 \\ C^k_{16} & C^k_{26} & C^k_{66} & 0 & C^k_{36} & 0 & 0 \\ -\lambda^k_1 & -\lambda^k_2 & 0 & -\left(\dfrac{\rho C}{\theta_{\text{ref}}}\right)^k & -\lambda^k_3 & 0 & 0 \\ C^k_{13} & C^k_{23} & C^k_{36} & -\lambda^k_3 & C^k_{33} & 0 & 0 \\ 0 & 0 & 0 & 0 & 0 & C^k_{55} & C^k_{45} \\ 0 & 0 & 0 & 0 & 0 & C^k_{45} & C^k_{44} \end{pmatrix}. \tag{29}$$

3.3. Through-the-thickness assumptions of primary variables

The behavior of primary unknowns $\boldsymbol{U}^k$ is postulated in the thickness plate z-directions according to a given expansion,

$$\boldsymbol{U}^k(x, y, z)=F_\tau(z)\boldsymbol{U}^k_\tau(x, y), \quad \tau=0, 1, \ldots, N, \tag{30}$$

while for virtual variations:

$$\delta\boldsymbol{U}^k(x, y, z)=F_s(z)\delta\boldsymbol{U}^k_s(x, y), \quad s=0, 1, \ldots, N. \tag{31}$$

The repeated indexes are summed over their ranges. Since superscript k appears in the vectors of primary unknowns and intensive variables, an LW theory is implied by the kinematic description (leaving superscript k form $\boldsymbol{U}$ and $\mathscr{E}$ leads to an ESL modeling). The polynomials $F_\tau(z)$ constitute a set of independent functions and N denotes the order of the introduced expansion. By appropriately choosing the thickness functions, both ESL and LW descriptions along the thickness of the plate are admissible. In an ESL model, a global assumption for the unknowns is considered along the thickness of the plate (i.e. a Taylor expansion) while, in an LW model, the expansion is made for each layer separately (employing Lagrange or Legendre polynomials). The interlaminar continuity conditions are enforced by the assembly procedure. The LW description leads generally to more accurate results but the number of the nodal degrees of freedom increases with the number of the

DOI: 10.1002/nme

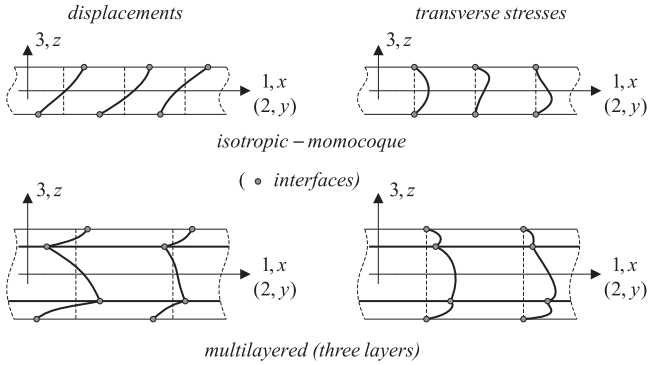

Figure 1. Displacement and transverse stress distribution in the plate thickness direction z. Comparison between a one-layered and a three-layered plate structure.

layers coming out to a greater computational cost. The above expansion is made according to the CUF [23], which permits to write in a unified form a large variety of plate theories.

3.4. Finite element discretization

In case of FEM implementation, unknowns and virtual variations can be expressed in terms of their nodal values, via the shape functions N_i:

$$\boldsymbol{U}_{\tau}^{k}(x,y) = N_i(x,y)\boldsymbol{Q}_{\tau i}^{k}, \quad i = 1,2,\ldots,N_n, \tag{32}$$

$$\delta\boldsymbol{U}_{s}^{k}(x,y) = N_j(x,y)\delta\boldsymbol{Q}_{sj}^{k}, \quad j = 1,2,\ldots,N_n, \tag{33}$$

where N_n denotes the number of nodes of the considered finite element and $\boldsymbol{Q}_{\tau i}^{k}$ is the vector of the nodal values of the primary unknowns:

$$\boldsymbol{Q}_{\tau i}^{k\mathrm{T}} = \{Q_{u_1\tau i}^{k} \quad Q_{u_2\tau i}^{k} \quad Q_{u_3\tau i}^{k} \quad Q_{\theta\tau i}^{k}\}. \tag{34}$$

Substituting Equations (32), (33) into Equations (30), (31), the final expression of primary unknowns can be obtained:

$$\boldsymbol{U}^{k}(x,y,z) = F_{\tau}N_i\boldsymbol{Q}_{\tau i}^{k}. \tag{35}$$

3.5. Fundamental nuclei and FE matrices

Substituting Equations (26), (28), (30) and (32) into the variational statement of Equation (23) leads to a set of equilibrium equations which can be formally put in the following compact form:

$$\delta\boldsymbol{Q}_{sj}^{k}: \quad \boldsymbol{M}^{k\tau sij}\ddot{\boldsymbol{Q}}_{\tau i}^{k} + \boldsymbol{K}^{k\tau sij}\boldsymbol{Q}_{\tau i}^{k} = \boldsymbol{P}_{sj}^{k}, \tag{36}$$

where $\boldsymbol{P}^{k}$ is the vector of external loads. The related boundary conditions can be expressed by $\overline{\boldsymbol{Q}}^{k}$.

The number of obtained equations coincides with the number of introduced variables: τ and s vary from 0 to N, i and j vary from 1 to N_n and k ranges from 1 to N_l. Matrix $\boldsymbol{K}^{k\tau sij}$ is the so-called stiffness fundamental nucleus. It is a 4×4 array and it provides the information to build the stiffness matrix. Matrix $\boldsymbol{M}^{k\tau sij}$ represents the fundamental nucleus related to the mass matrix. The fundamental nuclei are listed in an explicit form in the Appendix. Moreover, it is illustrated how to customize the fundamental nucleus in order to obtain the thermo-mechanical instantaneous solution or the steady-state result, when thermal loading is applied.

Starting from the fundamental nuclei, for a given discretization, the mass matrix $\boldsymbol{M}$ and the stiffness matrix $\boldsymbol{K}$ can be calculated by a numerical integration and the assembly procedure. The selective integration is used to overcome the shear-locking problem. These two matrices are representative of inertial and Gibbs free energy contributions, respectively. It should be emphasized

DOI: 10.1002/nme

that the stiffness matrix contains information pertaining to the mechanical and the thermal fields. On the contrary, the mass matrix only concerns the mechanical field.

The undamped dynamic problem can now be written in terms of the following ordinary differential equations system:

$$\boldsymbol{M}\ddot{\boldsymbol{Q}}+\boldsymbol{K}\boldsymbol{Q}=\boldsymbol{F}, \tag{37}$$

where:

$\boldsymbol{Q}$ is the vector of nodal primary unknowns;
$\ddot{\boldsymbol{Q}}$ is the vector of nodal accelerations;
$\boldsymbol{F}$ is the vector of nodal loads.

Moreover, the ith natural frequency of the system ω_i can be calculated by solving the generalized eigenvalues problem:

$$(-\omega_i^2\boldsymbol{M}+\boldsymbol{K})\boldsymbol{a}_i=\boldsymbol{0}, \tag{38}$$

where $\boldsymbol{a}_i$ is the ith eigenvector.

If a static analysis is required, the system to solve is the following:

$$\boldsymbol{K}\boldsymbol{Q}=\boldsymbol{F}. \tag{39}$$

Such system can be solved taking into account the boundary conditions $\overline{\boldsymbol{Q}}_\Gamma^k$, which are related to the various fields addressed in the analysis.

Acronyms are used for the implemented plate elements. These are denoted by LD1, LD2, LD3, LD4 in which: L states that an LW description is employed and D indicates that the PVD is applied; 1–4 denotes the order of the thickness expansion introduced for the field variables (from first to fourth order). When acronyms ED1, ED2, ED3, ED4 are used, the equivalent-single-layer description is employed.

4. NUMERICAL RESULTS

The set of FEs proposed in this paper has been implemented in the academic computational tool called MUL2 (modeling for MULtilayered structures in MULtifield approach). The results are illustrated and discussed in the following through comparisons with exact solutions.

4.1. Pure mechanical assessments

4.1.1. Convergence study (*static analysis*). A three-layer thin square plate of unitary side ($a=1$(m)) loaded by a sinusoidal unitary pressure at the top face ($\widehat{p}_z=1\,(\mathrm{N/m^2})$) is considered. The plate is simply supported at the two opposite sides with zero pressure (cylindrical bending). The layers are of equal thickness and they are made of the same orthotropic material. The total thickness ratio is $a/h=100$ and the lamination scheme is [0/90/0]. Material properties are: $E_1=25$, $E_2=1$, $E_3=1$, $G_1=0.5$, $G_2=0.5$, $G_3=0.2$ (all in (GPa)); $\nu_{12}=0.25$, $\nu_{13}=0.25$, $\nu_{25}=0.25$. As the plate is very thin, the reduced integration technique has been preserved to overcome the shear locking phenomena. The convergence results concerning the midplane transverse displacement at the center of the plate are shown in Figure 2 for LDn and EDn Q4 FEs (Q4 stands for four-node Quadrangular finite elements). Regular $n\times 1$ meshes are considered. Following remarks can be made. LDn FEs have good convergency properties. Simple FEs such as ED1 and ED2 converge to a value different from the exact solution, even when calculating a displacement. This error decreases as the order of the thickness expansion increases.

4.1.2. Convergence study (*mode analysis*). An isotropic, simply supported, square plate ($a=b=$ 0.3 (m), $t=0.0032$ (min), $E=210E9$ ($\mathrm{N/m^2}$), $\nu=0.3$ and $\rho=7860$ ($\mathrm{Kg/m^3}$)) is considered under the linear mode analysis. The undamped natural frequencies are calculated in MSC/Nastran and

DOI: 10.1002/nme

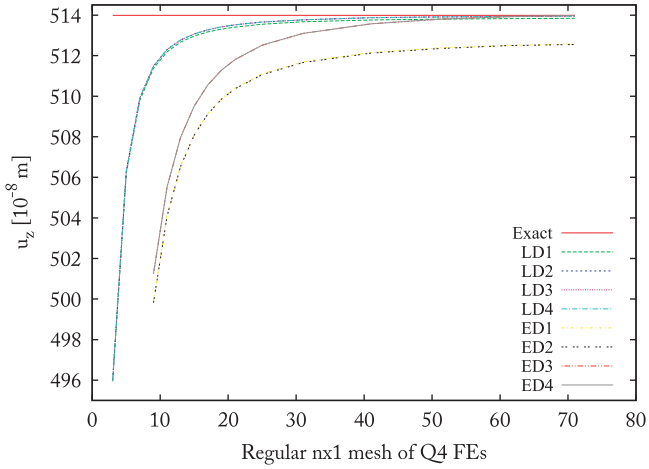

Figure 2. Midplane transverse displacement at the center of the plate: convergence study.

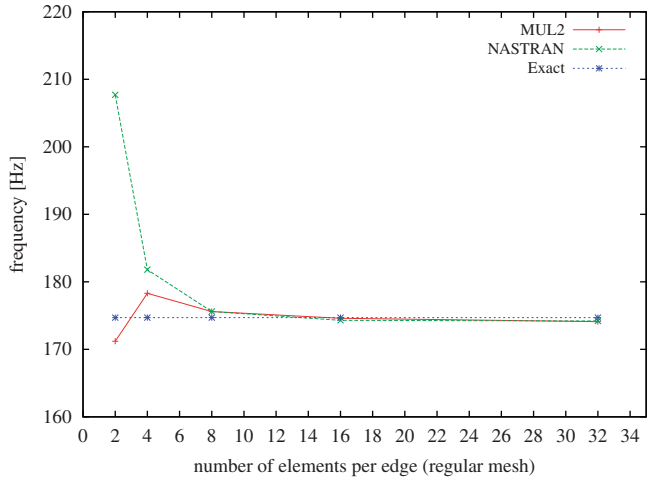

Figure 3. Convergence study for the first undamped natural frequency.

MUL2 SW according to the ESL Mindlin plate theory (ED1 FEs) and they are compared with the closed-form solution. The simply supported edge condition is defined by setting the three translations to zero at a boundary node. Regular $n \times n$ meshes of Q4 FEs are employed. Figure 3 shows good convergence properties. In particular, as the mesh is refined beyond 16×16, the FEM analysis predicts a lower frequency than the exact value. This is because the exact frequency is based on the thin and not shear deformation plate theory.

4.2. Mechanical loading: static instantaneous thermo-mechanical analysis

A simply supported square aluminum plate is considered to investigate the 'full' coupling between temperature and mechanical fields. To the authors' best knowledge, no results are available on this topic. The reason for this absence lies on the fact that this type of coupling is negligible for those materials, which are normally employed in thermal structures. The analysis of a simple isotropic plate is proposed. The results are shown in a dimensional form so that numbers can be judged by engineering sense. The mechanical properties are: $E = 73$ (GPa), $\nu = 0.3$, $\alpha = 25\text{E}{-6}$ (K^{-1}), $C = 897$ (J/(kg K)), $\rho = 2800$ (kg/m^3). The plate dimensions are: length and width $a = b = 10$ (m), thickness $h = 1$ (m). The plate is loaded at the top face by the bi-sinusoidal pressure of peak

DOI: 10.1002/nme

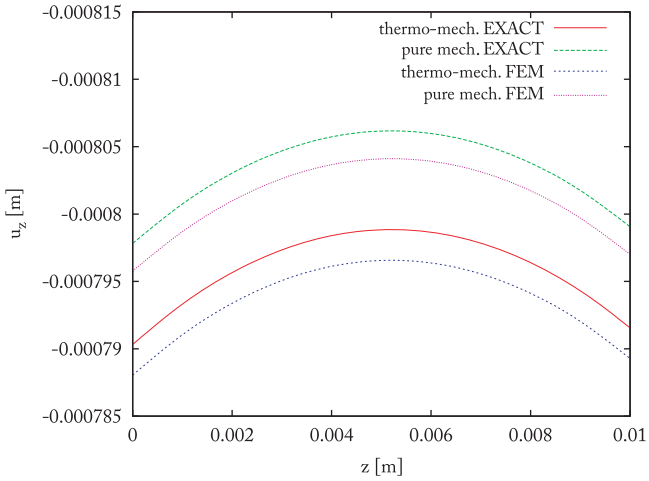

Figure 4. Through-the-thickness displacement at the plate position $\left(\frac{a}{2}, \frac{b}{2}\right)$—a regular 23×23 mesh of Q4 LD4 FEs is employed.

value $p_m = 2\text{E}7$ (Pa). Such load leads to a stress condition very close to the material elastic limit: $\sigma_{xx} = \sigma_{yy} \simeq 404\text{E}6$ (Pa). The present case study provides an example of the maximum thermal variation caused by a mechanical loading, within the frame of a linear static analysis. A 23×23 mesh of LD4 Q4 elements is employed. In general, there is no substantial difference in terms of displacements between those two analyses for displacements u_x and u_y. A slight difference can be seen in Figure 4, where the transverse displacement u_z is plotted along the z-axis, which has the origin is at the bottom of the plate. The difference between this two analyses is very small and it is due to the fact that for a fully coupled thermo-mechanical analysis, a small part of the work is employed to modify the temperature of the plate. The u_z displacement for this kind of analysis is smaller than the one obtained by a simple mechanical analysis, because a part of the work is used to develop the temperature variation. The same amount of work is subtracted from the work used to deform the plate. It can be seen that only a small part of work has been used to modify the temperature. In fact, Figure 5 shows that the maximum thermal variation is lower than 2.5 (K) (with the stresses close to the elastic limit). Figure 6 gives a three-dimensional representation of the thermal field calculated at the top/bottom face of the plate (the thickness axis is scaled unequally to make the temperature field more visible). It is implicit that the calculated temperature profile concerns the first moment in which the *static* load is applied to the structure. In fact, after the transient heat change in the plate itself, the temperature variation would be equal to zero throughout the plate and the displacement field will become the one calculated in a pure mechanical analysis.

To be remarked that, in accordance with the proposed approach, the inclusion of thermo-mechanical full coupling leads to the addition of one DOF at each row and column of the stiffness fundamental nucleus, with consequent increase in the computational time. The author experienced that solving a generic fully coupled static analysis by using direct methods requires almost twice than the corresponding pure mechanical problem. Additional efforts should be devoted to optimize the solver referring to iterative methods for sparse systems.

4.3. Thermal loading: higher order effects on displacements and stress results

In this section, several Q9 FEM results of thermo-mechanical static analysis of multilayered anisotropic plates obtained in MUL2 are compared with the 3D exact solutions found by Bhaskar and Varadan [11]. The numerical results are presented for the bending of a $(0^\circ/90^\circ/0^\circ)$ square $(a = b)$ laminate due to the temperature field given by

$$\theta = \overline{\theta}(2z/h) \sin\left(\frac{\pi x}{a}\right) \sin\left(\frac{\pi y}{b}\right), \tag{40}$$

DOI: 10.1002/nme

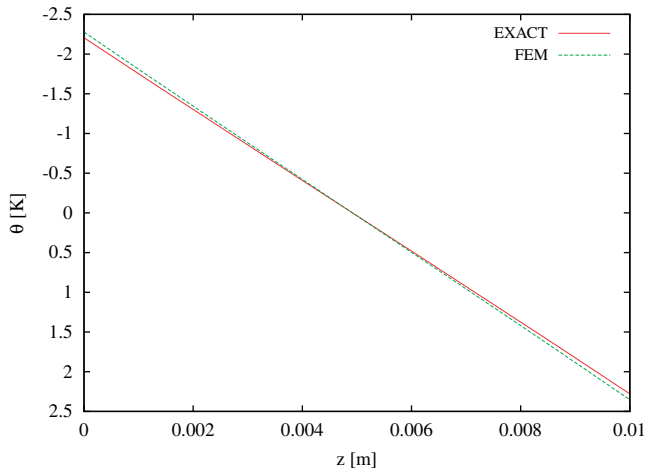

Figure 5. Through-the-thickness temperature profile at the plate position $\left(\frac{a}{2}, \frac{b}{2}\right)$—a regular 23×23 mesh of Q4 LD4 FEs is employed.

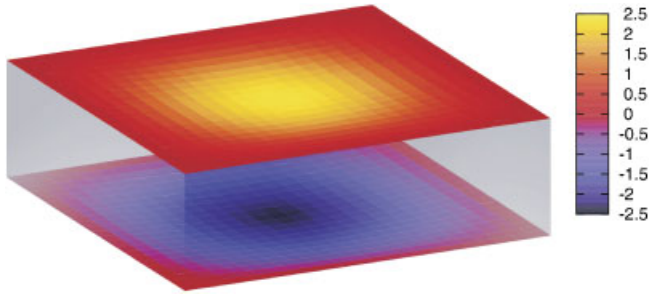

Figure 6. View of the plate under static deformation; the colors at the top and bottom faces indicate the instantaneous temperature variation—unit of measurement (K).

where h is the total thickness of the laminate and the origin of the z-axis is at the center of the plate. Different thickness ratios are considered, ranging from very thick ($a/h = 2$) to very thin ($a/h = 100$) plates. The following material properties, typical of high-modulus graphite/epoxy, are assumed:

$$E_L/E_T = 25,$$
$$G_{LT}/E_T = 0.5,$$
$$G_{TT}/E_T = 0.2,$$
$$\nu_{LT}/\nu_{TT} = 0.25,$$
$$\alpha_T/\alpha_L = 1125,$$

where L and T refer to the directions parallel and perpendicular, respectively, to the fibers. In the FEM analysis, the dimensional values given for material properties are thought to be coherent with the above given dimensionless ratios.

The distribution of temperature along the thickness, for given thermal boundary conditions at the top and at the bottom surfaces, can be obtained by a solution of the heat conduction equation (see, for example, the work of Tungikar and Rao [24]). However, only simple linear antisymmetric (with respect to z) thermal variation is considered as this would lead to bending (without stretching) of a

DOI: 10.1002/nme

symmetric laminate and would be adequate to bring out the importance of non-classical influences, such as shear deformation and thickness stretch.

The deflections and stresses are presented in terms of the following dimensionless parameters (sign$\widetilde{\ }$):

$$\widetilde{u}_z = \frac{u_z}{h\alpha_L \overline{\theta} \left(\frac{a}{h}\right)^2}, \quad (\widetilde{u}_x, \widetilde{u}_y) = \frac{(u_x, u_y)}{h\alpha_L \overline{\theta}(a/h)}, \quad \widetilde{\sigma}_{ij} = \frac{\sigma_{ij}}{E_T \alpha_L \overline{\theta}}.$$

In Tables I–IV there is a comparison between the 3D exact solution [11] and the FEM results obtained with the proposed thermo-mechanical FEs, with the through-the-thickness expansion ranging from one to four. Even if the employed mesh is not particularly refined, FEM results obtained with higher order thickness expansion (e.g. LD3/LD4) are in very good agreement with the exact solution, both for displacement and for in-plane stresses, wherever is the plate thickness ratio. On the other side, the results obtained by LD1 FEs are in general accurate only for thin multilayered plates. See the graphic view of Table I–IV in Figures 7–12. From these results it is deduced that when the plate is very thick, LD1 and LD2 modeling do not fully describe higher order/three-dimensional effects. In other words, low-order kinematic descriptions are not appropriate to analyze extremely thick plates. In order to better investigate this point, it can be noted that the available analytical solution for the LD1 (Table I, $a/h=4$) is different from the 3D result and hence the corresponding FE is not expected to converge to the 3D solution. The same reasoning can be applied for stress results (with amplified discrepancies). Figures 7–12 illustrate that rising the order of the kinematic description permits to approach 3D results also in case of very thick plates. A slight error in the convergence of FEM results could be due to the fact that some quantities are calculated on the plate edges, where boundary conditions are also applied.

Figures 13 and 14 show the convergence study respectively for $u_z\left(\frac{a}{2}, \frac{a}{2}, \frac{h}{2}\right)$ and $\sigma_{zz}\left(\frac{a}{2}, \frac{a}{2}, \frac{h}{2}\right)$, with $a/h=20$. It can be concluded that FEM results converge to the 3D exact values [11] and that accurate results for displacements and in-plane stresses are obtained with Q9 FEs, even with a poor mesh. Moreover, it is confirmed that the convergence is much faster for displacements than for stresses. Additional details on the thermo-mechanical coupling effect can be found in the previous work [25].

4.4. Thermal loading: assessment of temperature profile, steady-state solution

A simply supported three-layered square plate of edge $a=0.1$ (m) is considered. The top and bottom layers are made of aluminum, having equal thickness h_1. The middle layer is made of steel and has

Table I. z values are given in parentheses; (x, y) values are: $(a/2, a/2)$ for $\widetilde{u}_z$, $\widetilde{\sigma}_{xx}$ and $\widetilde{\sigma}_{yy}$; $(0, a/2)$ for $\widetilde{u}_x$; $(a/2, 0)$ for $\widetilde{u}_y$ and $(0, 0)$ for $\widetilde{\sigma}_{xy}$—a regular 6×6 mesh of Q9 LD1 FEs is employed.

$\frac{a}{h}$	Sol.	$\widetilde{u}_x\left(\mp\frac{h}{2}\right)$	$\widetilde{u}_y\left(\mp\frac{h}{2}\right)$	$\widetilde{u}_z\left(\mp\frac{h}{2}\right)$	$\widetilde{\sigma}_{xx}\left(\pm\frac{h}{2}\right)$	$\widetilde{\sigma}_{yy}\left(\mp\frac{h}{2}\right)$	$\widetilde{\sigma}_{xy}\left(\mp\frac{h}{2}\right)$
2	3D [11]	±20.04	±151.4	96.79	±1390	±635.4	±269.3
2	FEM	±12.14	±155.0	86.71	±643.4	±741.6	±268.6
4	3D [11]	±18.11	±81.83	42.69	±1183	±856.1	±157.0
4	Analytical [17]	—	—	41.24	—	—	—
4	FEM	±15.95	±84.05	40.95	±895.2	±965.3	±160.7
10	3D [11]	±16.61	±31.95	17.39	±1026	±1014	±76.29
10	FEM	±17.01	±33.02	17.61	±935.6	±1132	±80.46
20	3D [11]	±16.17	±20.34	12.12	±982.0	±1051	±57.35
20	FEM	±17.06	±21.32	12.66	±929.0	±1170	±61.75
50	3D [11]	±16.02	±16.71	10.50	±967.5	±1063	±51.41
50	FEM	±17.05	±17.70	11.14	±925.1	±1182	±55.87
100	3D [11]	±16.00	±16.17	10.26	±965.4	±1065	±50.53
100	Analytical [17]	—	—	10.92	—	—	—
100	FEM	±17.04	±17.19	10.91	±923.6	±1184	±54.97
CLT	EX. [11]	±15.99	±15.99	10.18	±964.6	±1065	±50.24

DOI: 10.1002/nme

Table II. z values are given in parentheses; (x, y) values are: $(a/2, a/2)$ for $\widetilde{u}_z$, $\widetilde{\sigma}_{xx}$ and $\widetilde{\sigma}_{yy}$; $(0, a/2)$ for $\widetilde{u}_x$; $(a/2, 0)$ for $\widetilde{u}_y$ and $(0, 0)$ for $\widetilde{\sigma}_{xy}$—a regular 6×6 mesh of Q9 LD2 FEs is employed.

$\frac{a}{h}$	Sol.	$\widetilde{u}_x\left(\mp\frac{h}{2}\right)$	$\widetilde{u}_y\left(\mp\frac{h}{2}\right)$	$\widetilde{u}_z\left(\mp\frac{h}{2}\right)$	$\widetilde{\sigma}_{xx}\left(\pm\frac{h}{2}\right)$	$\widetilde{\sigma}_{yy}\left(\mp\frac{h}{2}\right)$	$\widetilde{\sigma}_{xy}\left(\mp\frac{h}{2}\right)$
2	3D [11]	±20.04	±151.4	96.79	±1390	±635.4	±269.3
2	FEM	±16.77	±140.3	88.26	±1141	±675.0	±252.0
4	3D [11]	±18.11	±81.83	42.69	±1183	±856.1	±157.0
4	Analytical [17]	—	—	42.25	—	—	—
4	FEM	±17.47	±79.81	41.50	±1159	±860.3	±156.1
10	3D [11]	±16.61	±31.95	17.39	±1026	±1014	±76.29
10	FEM	±16.58	±31.77	17.32	±1052	±1013	±77.70
20	3D [11]	±16.17	±20.34	12.12	±982.0	±1051	±57.35
20	FEM	±16.19	±20.27	12.11	±1012	±1050	±58.62
50	3D [11]	±16.02	±16.71	10.50	±967.5	±1063	±51.41
50	FEM	±16.04	±16.67	10.50	±997.0	±1062	±52.57
100	3D [11]	±16.00	±16.17	10.26	±965.4	±1065	±50.53
100	Analytical [17]	—	—	10.26	—	—	—
100	FEM	±16.01	±16.16	10.26	±994.0	±1063	±51.65
CLT	EX. [11]	±15.99	±15.99	10.18	±964.6	±1065	±50.24

Table III. z values are given in parentheses; (x, y) values are: $(a/2, a/2)$ for $\widetilde{u}_z$, $\widetilde{\sigma}_{xx}$ and $\widetilde{\sigma}_{yy}$; $(0, a/2)$ for $\widetilde{u}_x$; $(a/2, 0)$ for $\widetilde{u}_y$ and $(0, 0)$ for $\widetilde{\sigma}_{xy}$—a regular 6×6 mesh of Q9 LD3 FEs is employed.

$\frac{a}{h}$	Sol.	$\widetilde{u}_x\left(\mp\frac{h}{2}\right)$	$\widetilde{u}_y\left(\mp\frac{h}{2}\right)$	$\widetilde{u}_z\left(\mp\frac{h}{2}\right)$	$\widetilde{\sigma}_{xx}\left(\pm\frac{h}{2}\right)$	$\widetilde{\sigma}_{yy}\left(\mp\frac{h}{2}\right)$	$\widetilde{\sigma}_{xy}\left(\mp\frac{h}{2}\right)$
2	3D [11]	±20.04	±151.4	96.79	±1390	±635.4	±269.3
2	FEM	±18.55	±142.3	90.33	±1300	±656.7	±257.8
4	3D [11]	±18.11	±81.83	42.69	±1183	±856.1	±157.0
4	Analytical [17]	—	—	42.68	—	—	—
4	FEM	±17.82	±80.42	41.92	±1191	±855.0	±157.8
10	3D [11]	±16.61	±31.95	17.39	±1026	±1014	±76.29
10	FEM	±16.61	±31.81	17.34	±1055	±1012	±77.82
20	3D [11]	±16.17	±20.34	12.12	±982.0	±1051	±57.35
20	FEM	±16.19	±20.28	12.11	±1012	±1050	±58.64
50	3D [11]	±16.02	±16.71	10.50	±967.5	±1063	±51.41
50	FEM	±16.04	±16.67	10.50	±997.1	±1062	±52.57
100	3D [11]	±16.00	±16.17	10.26	±965.4	±1065	±50.53
100	Analytical [17]	—	—	10.26	—	—	—
100	FEM	±16.01	±16.16	10.26	±994.1	±1063	±51.65
CLT	EX. [11]	±15.99	±15.99	10.18	±964.6	±1065	±50.24

thickness $2\times h_2$ (Figure 15). Aluminum material properties are $E=73.0$E9 (Pa), $G=27.239$E9 (Pa), $v=0.34$, $\alpha=25\cdot E-6$ (K^{-1}), $\kappa=180$ (W/(mK)), $\rho=2800$ (kg/m^3) and $C=897$ J/(Kkg), where α is the coefficient of thermal expansion. Steel coefficients are $E=210.0$E9 (Pa), $G=80.77$E9 (Pa), $v=0.3$, $\alpha=11.1$E-6 (K^{-1}), $\kappa=13$ (W/(mK)), $\rho=7860$ (kg/m^3), $C=450$ J/(K kg). The T_{ref} is set to 298.15 (K). A temperature variation with respect to T_{ref} is imposed at the top and at the bottom face of the panel: $+10$ (K) and -10 (K), respectively. A coupled thermo-mechanical static analysis was run with a regular mesh of 11×11 Q4 LD1 FEs to calculate the through-the-thickness temperature profile and the plate displacement caused by the imposed temperatures, at steady-state condition. The attention is restricted to the central point of the plate $\left(\frac{a}{2}, \frac{a}{2}\right)$. Each curve in Figure 16 shows a temperature profile along the thickness of the plate. Different geometrical configurations are considered by the variation of h_1 and h_2 mutual dimensions, keeping the same total thickness. The calculated temperatures profiles are in very good agreement with the exact solution obtained applying Fourier's law (interface points θ_{exact}). The middle plate displacement u_z is illustrated in Figure 17 for the various choices of h_1/h_2 ratios. The configuration of minimum

DOI: 10.1002/nme

Table IV. z values are given in parentheses; (x, y) values are: $(a/2, a/2)$ for $\widetilde{u}_z$, $\widetilde{\sigma}_{xx}$ and $\widetilde{\sigma}_{yy}$; $(0, a/2)$ for $\widetilde{u}_x$; $(a/2, 0)$ for $\widetilde{u}_y$ and $(0, 0)$ for $\widetilde{\sigma}_{xy}$—a regular 6×6 mesh of Q9 LD4 FEs is employed.

$\frac{a}{h}$	Sol.	$\widetilde{u}_x\left(\mp\frac{h}{2}\right)$	$\widetilde{u}_y\left(\mp\frac{h}{2}\right)$	$\widetilde{u}_z\left(\mp\frac{h}{2}\right)$	$\widetilde{\sigma}_{xx}\left(\pm\frac{h}{2}\right)$	$\widetilde{\sigma}_{yy}\left(\mp\frac{h}{2}\right)$	$\widetilde{\sigma}_{xy}\left(\mp\frac{h}{2}\right)$
2	3D [11]	±20.04	±151.4	96.79	±1390	±635.4	±269.3
2	FEM	±18.65	±142.4	90.40	±1309	±654.7	±258.4
4	3D [11]	±18.11	±81.83	42.69	±1183	±856.1	±157.0
4	Analytical [17]	—	—	42.69	—	—	—
4	FEM	±17.82	±80.44	41.92	±1191	±854.9	±157.8
10	3D [11]	±16.61	±31.95	17.39	±1026	±1014	±76.29
10	FEM	±16.61	±31.81	17.34	±1055	±1012	±77.82
20	3D [11]	±16.17	±20.34	12.12	±982.0	±1051	±57.35
20	FEM	±16.19	±20.28	12.11	±1012	±1050	±58.64
50	3D [11]	±16.02	±16.71	10.50	±967.5	±1063	±51.41
50	FEM	±16.04	±16.67	10.50	±997.1	±1062	±52.57
100	3D [11]	±16.00	±16.17	10.26	±965.4	±1065	±50.53
100	Analytical [17]	—	—	10.26	—	—	—
100	FEM	±16.01	±16.16	10.26	±994.1	±1063	±51.65
CLT	EX. [11]	±15.99	±15.99	10.18	±964.6	±1065	±50.24

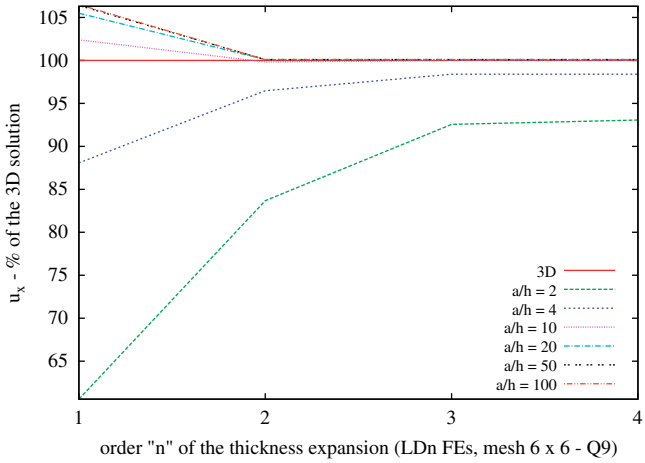

Figure 7. u_x: FEM results and 3D solution.

displacement is identified by the minimum of the curve. Figure 18 shows that the variation of the temperature profile when κ_2 varies progressively from the value typical of steel to the value typical of aluminum. The agreement with the exact solution is reconfirmed. Moreover, if $\kappa_1 = \kappa_2$ the temperature profile is linear, as usual for a single-layered panel. Figure 19 shows the variation of u_z for different κ_2/κ_1 ratios, with κ_1 kept constant. It is shown that the ideal configuration of maximum displacement is for $\kappa_2 = 0$. Moreover, as κ_2 increases, the displacement becomes minor (until an asymptotic value not present in the figure for reasons of scale).

A three-layered simply supported square plate with side $a = 0.1$ (m) and thickness ratio $a/h = 100$ is considered in the following. The external layers are made of aluminum, with thickness $h/4$. The internal layer is made of steel. The material properties are those listed for the above case study, with the only difference that $k = 80$ (W/(m K)) for the steel (difference introduced to make the figures more easy-to-read). The imposed θ is linear in the x and y directions: concerning the top surface of the plate: $\theta - \theta_{\text{ref}}$ starts from 0 (K), at point $(0, 0)$, and linearly increases along the bisector until 10 (K). Corresponding opposite values are imposed on the plate bottom surface (Figure 20). A coupled thermo-mechanical static analysis was run with a regular mesh of 11×11 Q4 LD1 FEs in order to calculate the steady-state temperature distribution in the plate. The temperature field

DOI: 10.1002/nme

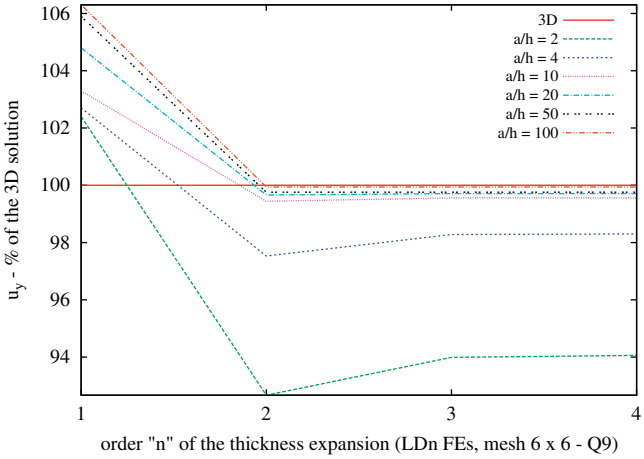

Figure 8. u_y: FEM results and 3D solution.

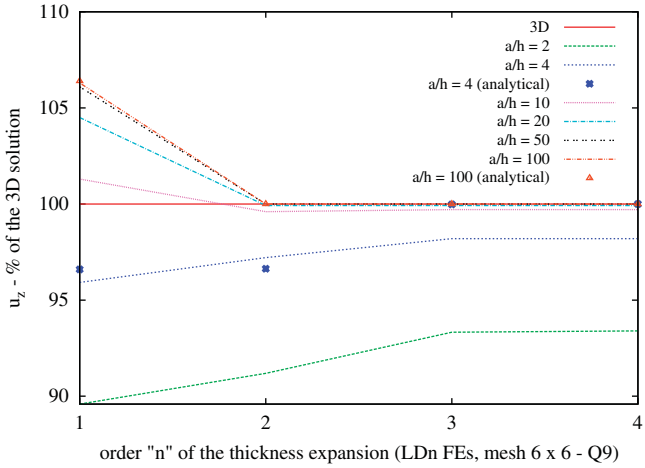

Figure 9. u_z: FEM results and 3D solution.

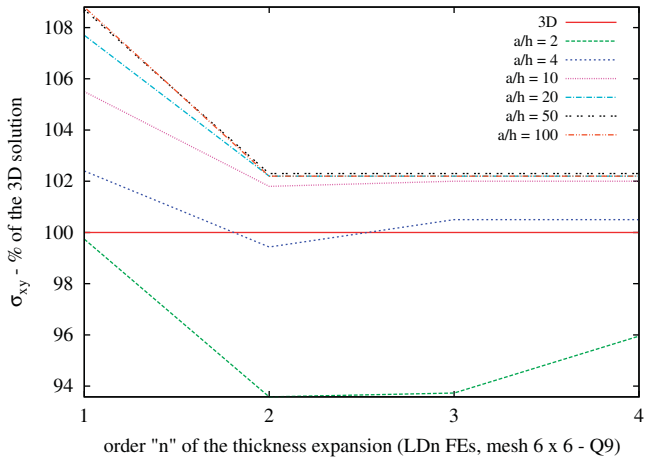

Figure 10. σ_{xy}: FEM results and 3D solution.

DOI: 10.1002/nme

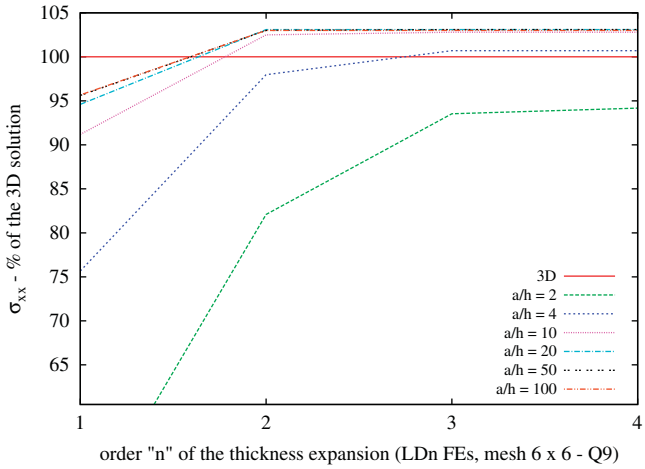

Figure 11. σ_{xx}: FEM results and 3D solution.

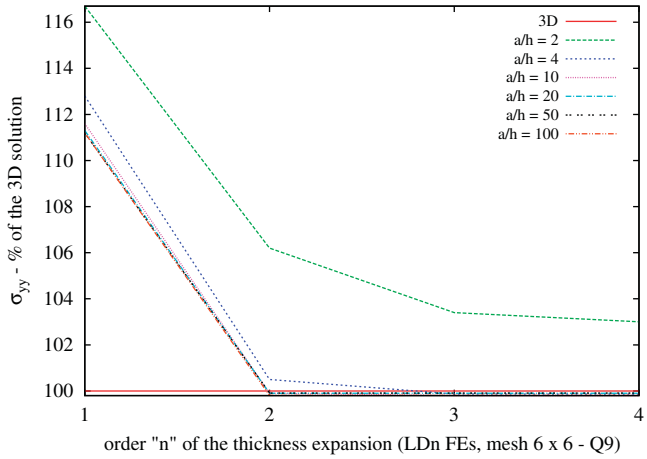

Figure 12. σ_{yy}: FEM results and 3D solution.

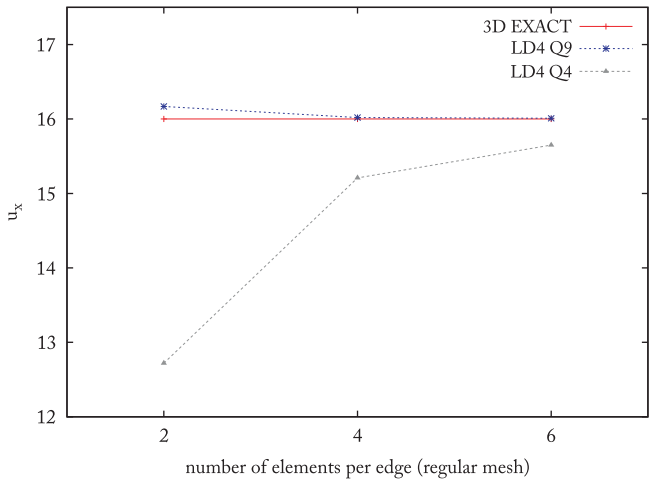

Figure 13. Convergence study for displacement u_x.

DOI: 10.1002/nme

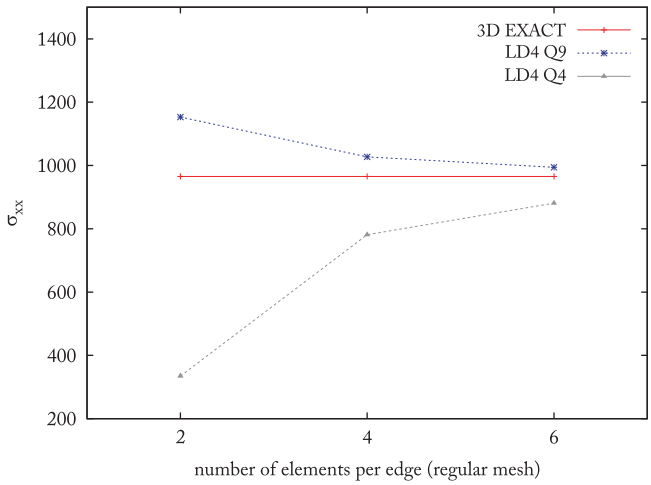

Figure 14. Convergence study for stress σ_{xx}.

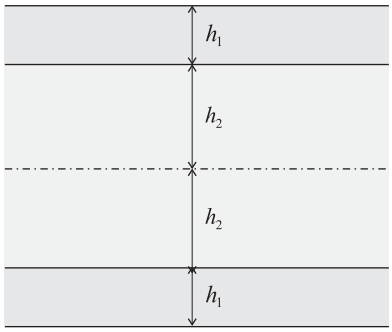

Figure 15. Plate-thickness geometry description.

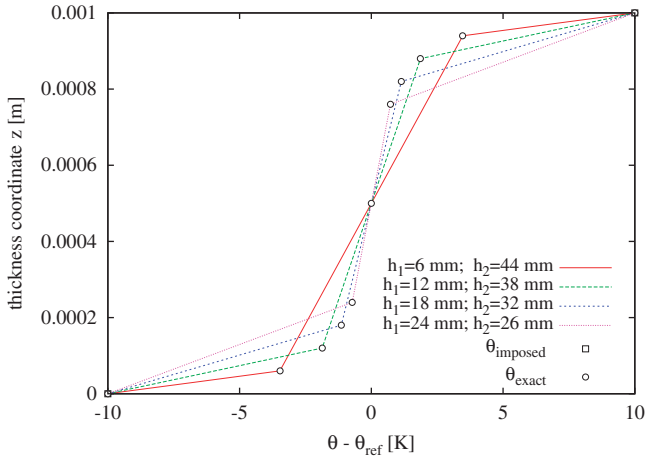

Figure 16. Variation of the plate-thickness temperature profile with the ratio h_1/h_2, total thickness constant—point $\left(\frac{a}{2}, \frac{a}{2}\right)$.

DOI: 10.1002/nme

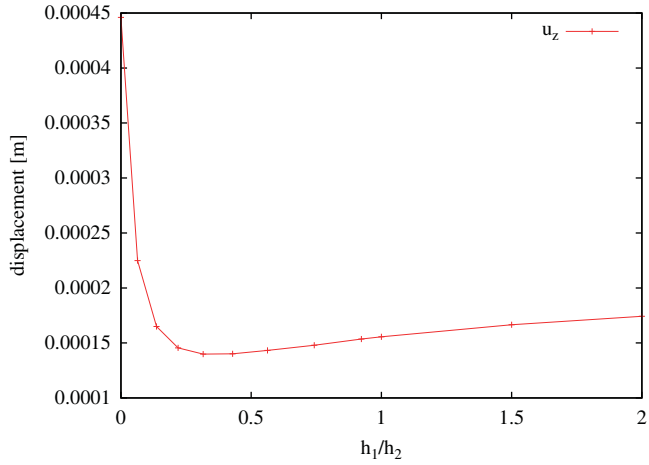

Figure 17. Variation of the displacement uz with the ratio h_1/h_2, total thickness constant—middle plate point.

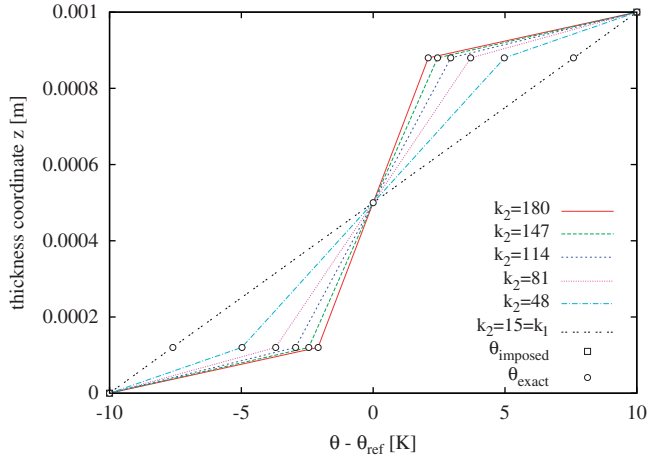

Figure 18. Variation of the plate-thickness temperature profile with the ratio κ_2/κ_1, κ_1 constant—point $\left(\frac{a}{2}, \frac{a}{2}\right)$.

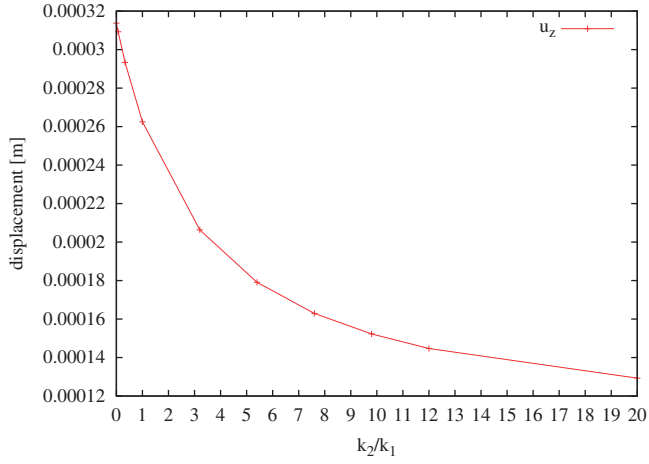

Figure 19. Variation of the displacement u_z with the ratio κ_2/κ_1, κ_1 constant—middle plate point.

DOI: 10.1002/nme

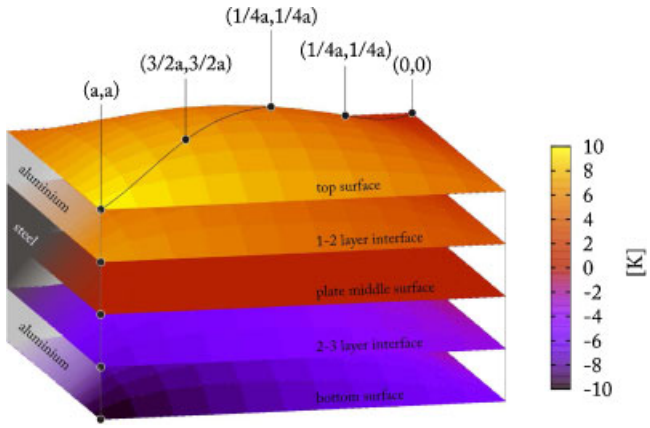

Figure 20. Temperature profile at the interfaces: $\theta - \theta_{\text{ref}}$.

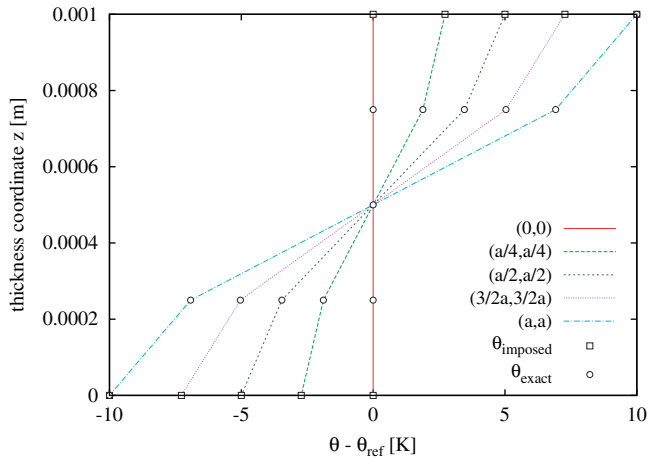

Figure 21. Plate-thickness temperature profile—locations indicated in Figure 20.

at the interfaces between layers is illustrated in Figure 20. The temperature variation at the plate middle surface is also plotted. This temperature distribution is clearly equal to zero, in accordance with the problem symmetry. The plate-thickness temperature profiles of five different locations are given in Figure 21. The good agreement with the Fourier's law is confirmed.

In conclusion, the case studies illustrated in this section show the usefulness of the formulated thermo-mechanical FEs, which permit to calculate in one single run the steady-state static deformation of a structure subjected to thermal loading. The separate application of the Fourier's law to obtain the through-the-thickness temperature profile is not required. In fact, the temperature distribution through all the layers of the structure is automatically calculated by using the material thermal conductivity coefficients, which are considered together with the other constitutive coefficients in the fundamental nucleus.

4.5. Thermo-mechanical dynamic analysis of aluminum plate

A mechanically fully clamped square plate of aluminum (material properties in Section 4.4) is considered with a regular 20×20 mesh of Q4 ED1 FEs. Two plate thickness ratios are considered: $1/10$ and $1/20$, with thickness equal to 0.01 and 0.005 (m), respectively. Pure mechanical and thermo-mechanical coupled cases are addressed. No mechanical or thermal preloading is considered. Thermo-mechanical mode shapes give the shape of the structure's

DOI: 10.1002/nme

Table V. Undamped natural frequencies calculated for the pure mechanical case and for the thermo-mechanical coupled case (Hz)—a regular 20×20 mesh of Q4 ED1 FEs is employed.

	Thickness ratio $= 1/10$			Thickness ratio $= 1/20$		
Freq. n	Pure mech.	Th.-mech.	Difference (%)	Pure mech.	Th.-mech.	Difference (%)
1	51740.9	52331.3	+1.14	27663.1	28018.1	+1.28
2	99963.2	100893	+0.93	55888.7	56513.3	+1.12
3	99963.2	101094	+1.13	55888.7	56649.8	+1.36
4	140360	141719	+0.97	81005.2	81986.6	+1.21
5	167999	168575	+0.34	99246.7	100378	+1.14
6	168310	168860	+0.33	99864.7	101075	+1.21
7	168310	169498	+0.71	121925	123248	+1.09

temperature distribution associated with corresponding natural frequencies, respecting the fact that compressed/expanded locations result hotter/colder respect to T_{ref}. In the time domain, the temperature variation of a fixed point would change sign alternatively and in accordance with the vibration frequency. In real cases, the change in temperature during vibration should be almost negligible. A more significant effect of coupling is described in Table V, where the comparison between the undamped natural frequencies calculated in the two analysis is presented. It can be noted that natural frequencies are sensitive to thermo-mechanical coupling effects. Moreover, the percentage difference depends not only on thermal coefficients but also, in small quantity, on the thickness ratio (and consequently on the impact of boundary conditions). As conclusion, aluminum can be considered as one of those materials that require the thermo-mechanical coupling in modeling, when very accurate results are needed for the plate analysis.

5. CONCLUSIONS

In this work, the PVD variational statement is applied to obtain multifield plate FEs for fully coupled thermo-mechanical analysis. Constitutive relations are obtained from a thermodynamic basis. A hierarchical approach is adopted to account for higher order effects when calculating the quantities through the plate-thickness direction. The order ranges from one to four. FEM matrices for static and dynamic problems are obtained starting from fundamental nuclei, in accordance with the CUF. Convergence studies, assessments and benchmarks are proposed both for pure mechanical and thermo-mechanical fully-coupled analysis. Higher order effects in the stress field calculation are quantified through comparisons with 3D solutions. The structure's stiffening due to the coupling between mechanical and thermal fields is described through the computation of undamped natural frequencies. The most innovative capability of the FEs proposed in this paper is the automatic calculation of the steady-state temperature profile through the thickness of the generic multilayered plate, when the thermal boundary conditions are imposed on the top and bottom surfaces. As a consequence, the separate application of Fourier's law to obtain the plate through-the-thickness temperature profile is no longer required and the steady-state static deformation/stress field of a structure under thermal loading can be calculated in one single run. All FEM results are obtained in the MUL2 academic code.

APPENDIX A: EXPLICIT FORMS OF PVD THERMO-MECHANICAL FUNDAMENTAL NUCLEI

The stiffness fundamental nucleus $\boldsymbol{K}^{k\tau sij}$ related to the PVD thermo-mechanical application is listed below. Constitutive information is included too. In the following, the layer-superscript k is always implied to simplify the equations.

DOI: 10.1002/nme

The stiffness fundamental nucleus is:

$$\boldsymbol{K}^{\tau sij} = \begin{bmatrix} K_{11} & K_{12} & K_{13} & K_{14} \\ K_{21} & K_{22} & K_{23} & K_{24} \\ K_{31} & K_{32} & K_{33} & K_{34} \\ K_{41} & K_{42} & K_{43} & K_{44} \end{bmatrix}. \tag{A1}$$

Its elements are:

$$\begin{aligned}
K_{11} &= C_{55}\lhd N_i N_j \rhd_\Omega \lessdot F_{\tau,z} F_{s,z} \gtrdot_z + C_{11}\lhd N_{i,x} N_{j,x} \rhd_\Omega \lessdot F_\tau F_s \gtrdot_z + C_{16}\lhd N_{i,y} N_{j,x} \rhd_\Omega \lessdot F_\tau F_s \gtrdot_z \\
&\quad + C_{16}\lhd N_{i,x} N_{j,y} \rhd_\Omega \lessdot F_\tau F_s \gtrdot_z + C_{66}\lhd N_{i,y} N_{j,y} \rhd_\Omega \lessdot F_\tau F_s \gtrdot_z \\
K_{21} &= C_{45}\lhd N_i N_j \rhd_\Omega \lessdot F_{\tau,z} F_{s,z} \gtrdot_z + C_{16}\lhd N_{i,x} N_{j,x} \rhd_\Omega \lessdot F_\tau F_s \gtrdot_z + C_{12}\lhd N_{i,y} N_{j,x} \rhd_\Omega \lessdot F_\tau F_s \gtrdot_z \\
&\quad + C_{66}\lhd N_{i,x} N_{j,y} \rhd_\Omega \lessdot F_\tau F_s \gtrdot_z + C_{26}\lhd N_{i,y} N_{j,y} \rhd_\Omega \lessdot F_\tau F_s \gtrdot_z + K_{31} \\
&= C_{55}\lhd N_{i,x} N_j \rhd_\Omega \lessdot F_\tau F_{s,z} \gtrdot_z + C_{45}\lhd N_{i,y} N_j \rhd_\Omega \lessdot F_\tau F_{s,z} \gtrdot_z + C_{13}\lhd N_i N_{j,x} \rhd_\Omega \lessdot F_{\tau,z} F_s \gtrdot_z \\
&\quad + C_{36}\lhd N_i N_{j,y} \rhd_\Omega \lessdot F_{\tau,z} F_s \gtrdot_z K_{41} = -\lambda_1 \lhd N_i N_{j,x} \rhd_\Omega \lessdot F_\tau F_s \gtrdot_z - \lambda_6 \lhd N_i N_{j,y} \rhd_\Omega \lessdot F_\tau F_s \gtrdot_z \\
K_{12} &= C_{45}\lhd N_i N_j \rhd_\Omega \lessdot F_{\tau,z} F_{s,x} \gtrdot_z + C_{16}\lhd N_{i,x} N_{j,x} \rhd_\Omega \lessdot F_\tau F_s \gtrdot_z + C_{66}\lhd N_{i,y} N_{j,x} \rhd_\Omega \lessdot F_\tau F_s \gtrdot_z \\
&\quad + C_{12}\lhd N_{i,x} N_{j,y} \rhd_\Omega \lessdot F_\tau F_s \gtrdot_z + C_{26}\lhd N_{i,y} N_{j,y} \rhd_\Omega \lessdot F_\tau F_s \gtrdot_z \\
K_{22} &= C_{44}\lhd N_i N_j \rhd_\Omega \lessdot F_{\tau,z} F_{s,z} \gtrdot_z + C_{66}\lhd N_{i,x} N_{j,x} \rhd_\Omega \lessdot F_\tau F_s \gtrdot_z + C_{26}\lhd N_{i,y} N_{j,x} \rhd_\Omega \lessdot F_\tau F_s \gtrdot_z \\
&\quad + C_{26}\lhd N_{i,x} N_{j,y} \rhd_\Omega \lessdot F_\tau F_s \gtrdot_z + C_{22}\lhd N_{i,y} N_{j,y} \rhd_\Omega \lessdot F_\tau F_s \gtrdot_z \\
K_{32} &= C_{45}\lhd N_{i,x} N_j \rhd_\Omega \lessdot F_\tau F_{s,z} \gtrdot_z + C_{44}\lhd N_{i,y} N_j \rhd_\Omega \lessdot F_\tau F_{s,z} \gtrdot_z + C_{36}\lhd N_i N_{j,x} \rhd_\Omega \lessdot F_{\tau,z} F_s \gtrdot_z \\
&\quad + C_{23}\lhd N_i N_{j,y} \rhd_\Omega \lessdot F_{\tau,z} F_s \gtrdot_z \\
K_{42} &= -\lambda_6 \lhd N_i N_{j,x} \rhd_\Omega \lessdot F_\tau F_s \gtrdot_z - \lambda_2 \lhd N_i N_{j,y} \rhd_\Omega \lessdot F_\tau F_s \gtrdot_z K_{13} \\
&= C_{13}\lhd N_{i,x} N_j \rhd_\Omega \lessdot F_\tau F_{s,z} \gtrdot_z + C_{36}\lhd N_{i,y} N_j \rhd_\Omega \lessdot F_\tau F_{s,z} \gtrdot_z + C_{55}\lhd N_i N_{j,x} \rhd_\Omega \lessdot F_{\tau,z} F_s \gtrdot_z \\
&\quad + C_{45}\lhd N_i N_{j,y} \rhd_\Omega \lessdot F_{\tau,z} F_s \gtrdot_z \\
K_{23} &= C_{36}\lhd N_{i,x} N_j \rhd_\Omega \lessdot F_\tau F_{s,z} \gtrdot_z + C_{23}\lhd N_{i,y} N_j \rhd_\Omega \lessdot F_\tau F_{s,z} \gtrdot_z + C_{45}\lhd N_i N_{j,x} \rhd_\Omega \lessdot F_{\tau,z} F_s \gtrdot_z \\
&\quad + C_{44}\lhd N_i N_{j,y} \rhd_\Omega \lessdot F_{\tau,z} F_s \gtrdot_z \\
K_{33} &= C_{33}\lhd N_i N_j \rhd_\Omega \lessdot F_{\tau,z} F_{s,z} \gtrdot_z + C_{55}\lhd N_{i,x} N_{j,x} \rhd_\Omega \lessdot F_\tau F_s \gtrdot_z + C_{45}\lhd N_{i,y} N_{j,x} \rhd_\Omega \lessdot F_\tau F_s \gtrdot_z \\
&\quad + C_{45}\lhd N_{i,x} N_{j,y} \rhd_\Omega \lessdot F_\tau F_s \gtrdot_z + C_{44}\lhd N_{i,y} N_{j,y} \rhd_\Omega \lessdot F_\tau F_s \gtrdot_z \\
K_{43} &= -\lambda_3 \lhd N_i N_j \rhd_\Omega \lessdot F_\tau F_{s,z} \gtrdot_z \\
K_{14} &= -\lambda_1 \lhd N_{i,x} N_j \rhd_\Omega \lessdot F_\tau F_s \gtrdot_z - \lambda_6 \lhd N_{i,y} N_j \rhd_\Omega \lessdot F_\tau F_s \gtrdot_z \\
K_{24} &= -\lambda_6 \lhd N_{i,x} N_j \rhd_\Omega \lessdot F_\tau F_s \gtrdot_z - \lambda_2 \lhd N_{i,y} N_j \rhd_\Omega \lessdot F_\tau F_s \gtrdot_z \\
K_{34} &= -\lambda_3 \lhd N_i N_j \rhd_\Omega \lessdot F_{\tau,z} F_s \gtrdot_z \\
K_{44} &= -\frac{\rho C \lhd N_i N_j \rhd_\Omega \lessdot F_\tau F_s \gtrdot_z}{\theta_{ref}}
\end{aligned}$$

Subscripts after comma indicates derivatives,

$$\lhd(.....)\rhd_\Omega = \int_{\Omega_k} (.....) \mathrm{d}\Omega_k \quad \text{and} \quad \lessdot(.....)\gtrdot_z = \int_{z_k} (.....) \mathrm{d}z_k.$$

DOI: 10.1002/nme

Non-zero elements of the mass fundamental nucleus $\boldsymbol{M}^{\tau sij}$ are:

$$M_{11} = M_{22} = M_{33} = M_{44} = M_{55} = \rho \lhd N_i N_j \rhd_\Omega \lessdot F_\tau F_s \gtrdot_z .$$

The fundamental nuclei showed above permit to calculate the instantaneous mechanical deformation and the temperature profile in the plate, when a mechanical/thermal loading is applied. The stiffness variation due to the thermo-mechanical coupling interactions is considered, while heat conduction and transient effects are not taken into account. In other words, the solution is the one valid at the initial time $t = 0$.

If a thermal loading is considered and the steady-state temperature profile is required, the cell K_{44} of $\boldsymbol{K}^{\tau sij}$ should be modified as the following:

$$K_{44} = -k_{33} \lhd N_i N_j \rhd_\Omega \lessdot F_{\tau,z} F_{s,z} \gtrdot_z - k_{22} \lhd N_{i,y} N_{j,y} \rhd_\Omega \lessdot F_\tau F_s \gtrdot_z - k_{11} \lhd N_{i,x} N_{j,x} \rhd_\Omega \lessdot F_\tau F_s \gtrdot_z .$$

ACKNOWLEDGEMENTS

This paper is supported by the European Space Agency, ESTEC under grant 21082/06/NL/PA.

REFERENCES

1. Thoronton EA. Thermal structures for aerospace applications. AIAA, Education Series. AIAA: Reston, VA, 1996.
2. Murakami H. Assessment of plate theories for treating the thermomechanical response of layered plates. *Composites Engineering* 1993; **3**(2):137–149.
3. Creschik G, Palisoc A, Cassapakis C, Veal G, Mikulas MM. Sensitivity study of precision pressurized membrane reflector deformations. *AIAA Journal* 2000; **38**:308–314.
4. Srinivas S, Rao AK. A note on flexture of thick rectangular plates and laminates with variation of temperature accross the thickness. *Bulletin of the Polish Academy of Sciences Series—Science and Technology* 1972; **20**: 229–234.
5. Bapu Rao MN. 3D analysis of thermally loaded thick plates. *Nuclear Engineering and Design* 1979; **55**:353–361.
6. Tungikar VB, Rao KM. Three dimensional exact solution of thermal stresses in rectangular composite laminate. *Composite Structures* 1994; **27**:419–427.
7. Bhaskar K, Varadan TK, Alii JSM. Thermoelastic solutions for orthotropic and anisotropic composite laminates. *Composites* 1996; **27B**:415–420.
8. Carrera E. A class of two dimensional theories for multilayered plates analysis. *Atti Accademia delle Scienze di Torino, Memorie Scienze Fisiche* 1995; **19–20**:49–87.
9. Bhaskar K, Varadan TK. A new theory for accurate thermal-mechanical flexural analysis of symmetric plates. *Composite Structures* 1999; **45**:227–232.
10. Carrera E, Brischetto S, Nali P. Variational statements and computational models for multifield problems and multilayered structures. *Special Issue of MAMS* 2008; **15**(3):182–198.
11. Bhaskar K, Varadan TK, Ali JSM. Thermoelastic solutions for orthotropic and anisotropic composite laminates. *Composites* 1996; **27**(5):415–420.
12. Rolfes R, Noor AK, Sparr H. Evaluation of transverse thermal stresses in composite plates based on first-order shear deformation theory. *Computer Methods in Applied Mechanics and Engineering* 1998; **167**:355–368.
13. Rolfes R, Noack J, Taeschner M. High performance 3D-analysis of thermo-mechanically loaded composite structures. *Composite Structures* 1999; **46**:367–379.
14. Rohwer K, Rolfes R, Sparr H. Higher-order theories for thermal stresses in layered plates. *International Journal of Solids and Structures* 2001; **38**:3673–3687.
15. Spiessberger C, Gleiter A, Busse G. Aerospace applications of lockin-thermography with optical, ultrasonic, and inductive excitation. *International Symposium on NDT in Aerospace*, Fürth, Germany, 2008.
16. Fantoni G, Merletti LG, Salerno A. Stato dell'arte della termografia Lock-In applicata a componenti di elicottero: analisi termoelastica e rilevazione di difetti. *Il Giornale Delle Prove Non Distruttive* 2008; (27):30–34.
17. Carrera E. An assessment of mixed and classical theories for the thermal stress analysis of orthotropic multilayered plates. *Journal of Thermal Stresses* 2000; **23**:797–831.
18. Robaldo A, Carrera E, Benjeddou A. Unified formulation for finite element. Thermoelastic analysis of multilayered anisotropic composite plates. *Journal of Thermal Stresses* 2005; **28**:1031–1065.
19. Robaldo A, Carrera E. Mixed finite elements for thermoelastic analysis of multilayered anisotropic plates. *Journal of Thermal Stresses* 2007; **30**(2):165–194.
20. Carrera E, Boscolo M, Robaldo A. Hierarchic multilayered plate elements for coupled multifield problems of piezoelectric adaptive structures: formulation and numerical assessment. *Composite Structures* 2007; **14**:383–430.
21. Ikeda T. *Fundamentals of Piezoelectricity*. Oxford Science Publications: Oxford, 1996.

DOI: 10.1002/nme

22. Altay GA, Dökmeci MC. Some variational principles for linear coupled thermoelasticity. *International Journal of Solids and Structures* 1996; **14**(26):3937–3948.
23. Carrera E. Developments, ideas and evaluations based upon the Reissner's mixed theorem in the modelling of multilayered plates and shells. *Applied Mechanics Review* 2001; **54**:301–329.
24. Tungikar VB, Rao KM. Three dimensional exact solution of thermal stresses in rectangular composite laminate. *Composite Structures* 1994; **27**:419–430.
25. Carrera E, Boscolo M, Robaldo A. Hierarchic multilayered plate elements for coupled multifield problems of piezoelectric adaptive structures: formulation and numerical assessment. *Archives of Computational Methods in Engineering* 2007; **14**:383–430.

DOI: 10.1002/nme